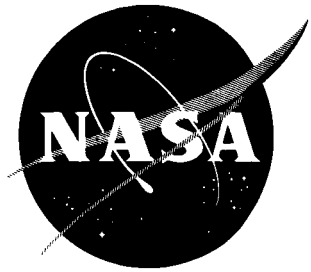

TECHNICAL NOTE

D-1788

EFFECT OF AERODYNAMIC HEATING ON THE FLUTTER OF THIN FLAT-PLATE ARROW WINGS

By Joseph M. Groen and Richard Rosecrans

Langley Research Center
Langley Station, Hampton, Va.

NATIONAL AERONAUTICS AND SPACE ADMINISTRATION
WASHINGTON

May 1963

Code-1

NATIONAL AERONAUTICS AND SPACE ADMINISTRATION

TECHNICAL NOTE D-1788

EFFECT OF AERODYNAMIC HEATING ON THE FLUTTER OF THIN FLAT-PLATE ARROW WINGS

By Joseph M. Groen and Richard Rosecrans

SUMMARY

Flutter tests were made on thin flat-plate aluminum arrow wings in a heated wind tunnel at a Mach number of 3. From the results of the tests, an experimental flutter boundary was obtained which showed the effect of aerodynamic heating. Induced thermal stress resulted in a loss of wing stiffness which lowered the flutter-velocity index by as much as one-third. The flutter boundary obtained also indicated the transient nature of the phenomenon.

Test results are compared with calculated values of temperature and with natural frequencies of vibration and associated nodal patterns. Measured flutter points are compared with a calculated flutter boundary for an unheated wing.

INTRODUCTION

The use of thin, low-aspect-ratio airfoils on supersonic aircraft and missiles has created a need for information concerning the aerothermoelastic behavior of such structures. It has been known for some time that airfoils subjected to aerodynamic heating, or any form of nonuniform heating which induces thermal stress, can experience a transient reduction in overall stiffness which makes them more susceptible to flutter. (See refs. 1 to 3.) Only limited experimental data are available which show the effects of both thermal and aerodynamic loadings on wing flutter. Proven theoretical methods for determining the extent of the change in flutter characteristics due to thermal stress are not presently available.

In this investigation, a series of wind-tunnel tests at elevated temperature was performed on solid models of one thickness, and of the same material and planform, to establish a flutter boundary. Four additional tests were made on models of a thicker wing to probe the effect of aerodynamic heating on the flutter of models scaled to a higher stiffness level. The tests were made in the Langley 9- by 6-foot thermal structures tunnel. The experimental results were used to evaluate the accuracy of existing procedures for the determination of temperatures and natural modes and frequencies of vibration. Measured flutter points were compared with a calculated flutter boundary for an unheated wing.

Temperature distributions were computed over the entire wing surface as a function of time, and the results were compared with experimental temperatures. Natural modes and frequencies of vibration of the unheated wings were calculated by the method of reference 4 and compared with measured frequencies and nodal patterns. The calculated modes and frequencies, along with piston-theory aerodynamics, were then used as input data for computing a flutter boundary by the method of reference 5.

SYMBOLS

A	cross-sectional area of a heat conduction element
b	semichord at 75-percent-span station
c	specific heat
f	cyclic frequency
h	aerodynamic heat-transfer coefficient
k	thermal conductivity of air
k_w	thermal conductivity of wing material
l	center-to-center length of a heat conduction path
N_{Pr}	Prandtl number
N_{Re}	Reynolds number
S	surface area of a heat conduction element
s	Rubesin correction factor
T	temperature at start of a time interval
T'	temperature at end of a time interval
T_{aw}	adiabatic wall temperature
T_e	local air temperature at outer edge of boundary layer
T_r	recovery temperature
T_w	temperature of wing material
ΔT	temperature rise above ambient starting temperature

t thermal thickness of wing (equals one-half actual thickness)

V velocity

x distance from wing leading edge parallel to airstream

μ mass-density parameter, mass of wing divided by mass of a conical volume of air enclosing the wing

ρ density of wing material

τ time

ω_α calculated (unless otherwise noted) circular frequency of third natural mode of vibration

Subscripts:

m refers to any element adjacent to element n

n refers to any element 1 through 50 (see fig. 6)

m-n refers to a boundary between elements m and n

t refers to a stagnation condition

$1,2,\ldots$ refers to natural modes of vibration in order of occurrence

MODELS, APPARATUS, AND TESTS

Wing Models

The models were wings of arrow planform with a solid cross-sectional area having beveled leading and trailing edges as shown in figure 1(a). They were constructed from 2024-T3 aluminum-alloy plates of two thicknesses, 0.125 and 0.156 inch, with a root chord of 25.50 inches and a semispan of 12.75 inches. The wings had an aspect ratio of 2. The included angle between the leading and trailing edges was approximately 14°. Some preliminary wind-tunnel tests indicated the presence of thermal buckling along the leading edge, which was then confirmed by radiant-heating tests. Consequently, the leading edge of each wing was modified by five 1-inch-deep sawcuts, at 4-inch intervals, perpendicular to the leading edge, to relieve the thermal-stress concentrations.

The wings were supported rigidly along their entire root chord by 1-inch-thick steel angles. The support approximated an infinite heat sink which permitted no thermal expansion in the clamped area. Connection details are shown in figure 1(b).

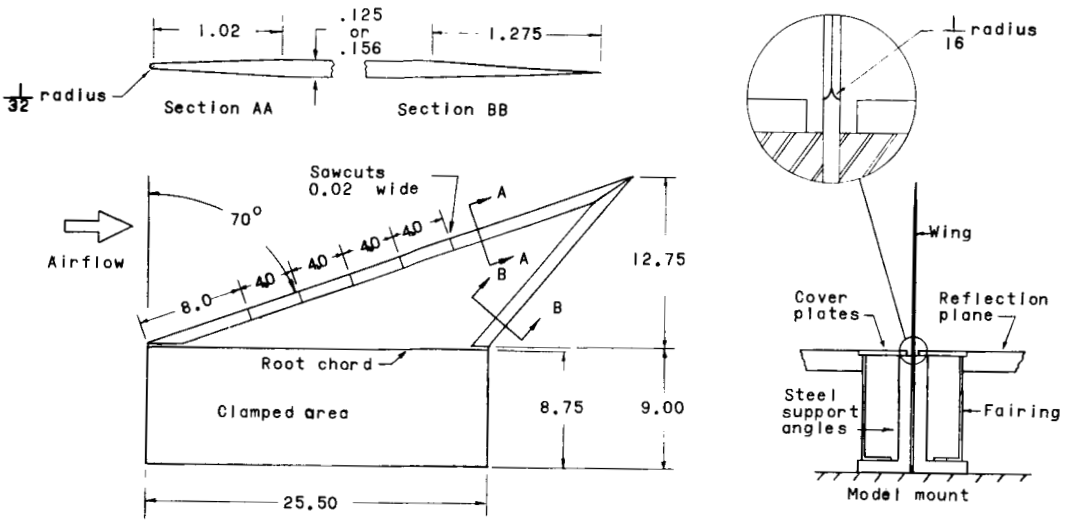

(a) Wing geometry.

(b) Root support.

Figure 1.- Wing model details. Linear dimensions are in inches.

Fourteen wing models were used in this investigation; ten were 0.125 inch thick and four were 0.156 inch thick. The 0.125-inch-thick models are designated wings A1 to A10 and the 0.156-inch-thick models are designated wings B1 to B4.

Instrumentation

Each wing was instrumented with thermocouples and strain gages located according to the master instrumentation diagram shown in figure 2. Three wings were instrumented completely; other wings utilized lesser amounts of instrumentation, but always at the locations shown.

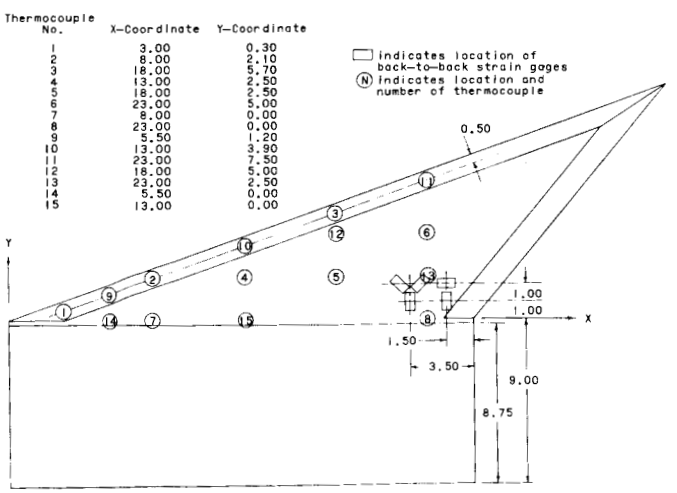

Figure 2.- Location of instrumentation. Linear dimensions are in inches.

The thermocouples were of iron-constantan, No. 36 wire, formed to a bead and spot-welded to the wing surface. Individual lead wires were cemented to the wing in a direction perpendicular to the leading edge toward the root. After the wires were cemented in place they were faired over with silicone rubber to minimize disturbance of the airflow.

Bakelite strain gages, placed back-to-back on opposite sides of the wing and wired into double-active-arm bridge circuits, were cemented just above the wing root

near the trailing edge as shown in figure 2. These gages were not intended to determine stresses, but were used only to record vibration frequencies during the wind-tunnel tests.

High-speed motion-picture cameras running at 1,000 frames per second were operated in sequence to record model behavior. The motion pictures were used in conjunction with the strain-gage records to determine test results.

Vibration Characteristics

Two separate measurements were made to determine the natural vibration frequencies of the wings, and the results are presented in table I. An air-jet

TABLE I.- NATURAL VIBRATION FREQUENCIES OF TEST MODELS

Wing	Frequency, in cps, for -							
	Models clamped in testing machine (semispan, 12.75 in.)					Models mounted in tunnel (semispan, 13.00 in.)		
	Mode 1	Mode 2	Mode 3	Mode 4	Mode 5	Mode 1	Mode 2	Mode 3
0.125-inch-thick wings								
A1	----	---	---	---	---	25.6	---	---
A2	27.3	91	147	210	253	26.1	---	---
A3	27.5	89	146	209	255	25.8	84	140
A4	27.5	91	148	211	253	26.6	85	142
A5	26.7	90	146	208	255	26.6	85	142
A6	----	---	---	---	---	24.4	80	133
A7	----	---	---	---	---	26.0	84	140
A8	27.5	88	144	206	252	25.4	83	139
A9	27.4	88	144	208	253	25.6	82	138
A10	27.6	88	144	207	250	25.5	83	138
Average	27.4	89	146	208	253	25.8	83	139
Calculated	27.0	88	142	202	253	----	---	---
0.156-inch-thick wings								
B1	35.3	116	188	268	326	33.7	---	---
B2	----	---	---	---	---	33.3	106	---
B3	35.5	118	191	275	330	33.3	108	180
B4	34.8	114	187	267	324	33.3	108	180
Average	35.2	116	189	270	327	33.4	107	180
Calculated	32.3	110	176	254	314	----	---	---

shaker was used to excite the wings. Resonance was determined by means of two electrical displacement-measuring coils, one mounted to determine the frequency output of the shaker and the other to determine the frequency response of the wing. The signals from the coils were fed into the X- and Y-axes of an oscilloscope, and at resonance a Lissajous ellipse was formed. Frequencies were measured by a Stroboconn frequency meter.

The first set of measurements was obtained with the wings clamped in a testing machine. For these tests, the wing semispan was 12.75 inches and there were no sawcuts in the leading edges. Nodes were obtained during these tests by sprinkling salt on the vibrating wing. The first five natural frequencies and nodal patterns were obtained. The second set of measurements was made just prior to testing, with the wings mounted in the tunnel test section. For these measurements, the wing semispan was 13.00 inches and the leading edge was segmented by sawcuts. Only the first three natural frequencies were obtained.

In order to separate the effect upon frequency of the leading-edge sawcuts from that due to the change in span, one model (wing A9) was subjected to further vibration tests. The wing was clamped in the testing machine, first with a variation in span, and then with a variation in leading-edge condition. The results are as follows for the first five frequencies:

Span, in.	Sawcuts	Frequency, in cps, for -				
		Mode 1	Mode 2	Mode 3	Mode 4	Mode 5
13.00	No	26.8	84.8	140.8	201.7	244.7
12.75	No	27.4	87.8	143.5	208.2	252.7
12.75	Yes	27.5	87.8	144.3	205.6	251.0

The effect of a change in span is seen to be large in comparison with the effect of the sawcuts. Root clamping forces between 10,000 and 60,000 pounds did not affect the frequencies. All data were therefore obtained with a root clamping force of 30,000 pounds. The models were made from commercial aluminum sheets which varied in thickness by as much as 3 percent. Consequently, the same wing was used for all the frequency measurements tabulated above so that no errors would be introduced by differences in wing thickness. It should be noted that this variation in thickness can account for some of the scatter in the test data where more than one model is involved.

Natural modes and frequencies of vibration were calculated for a 0.125-inch-thick wing by the method of reference 4, and the frequencies are given in table I A short discussion of the method is given in the appendix. A span of 12.75 inche was used in the calculations; therefore, calculated frequencies should be compared with measured values for the same span. Agreement is seen to be good. Mode shapes for the first four modes are shown in figure 3. From the mode shapes node lines were established and compared with experimental nodes in figure 4. The calculated nodal patterns are seen to be similar to the measured patterns for all modes. With both the nodes and frequencies in good agreement, it seems reasonable to place confidence in the accuracy of the modal displacements at points not on node lines. Such a conclusion was substantiated by a number of additional calculations and measurements for wings of different thickness, material, and planform which gave similarly good agreement for both frequencies and nodal patterns.

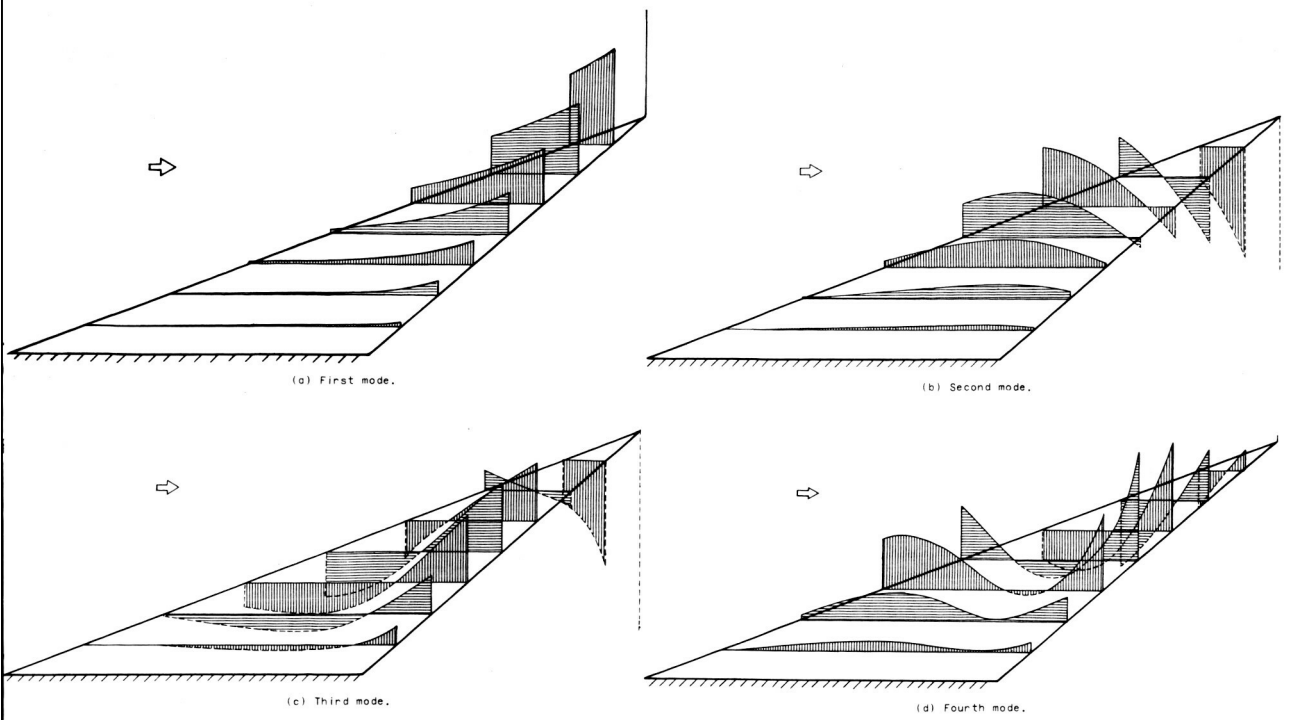

Figure 3.- Calculated natural modes for a 0.125-inch-thick arrow wing.

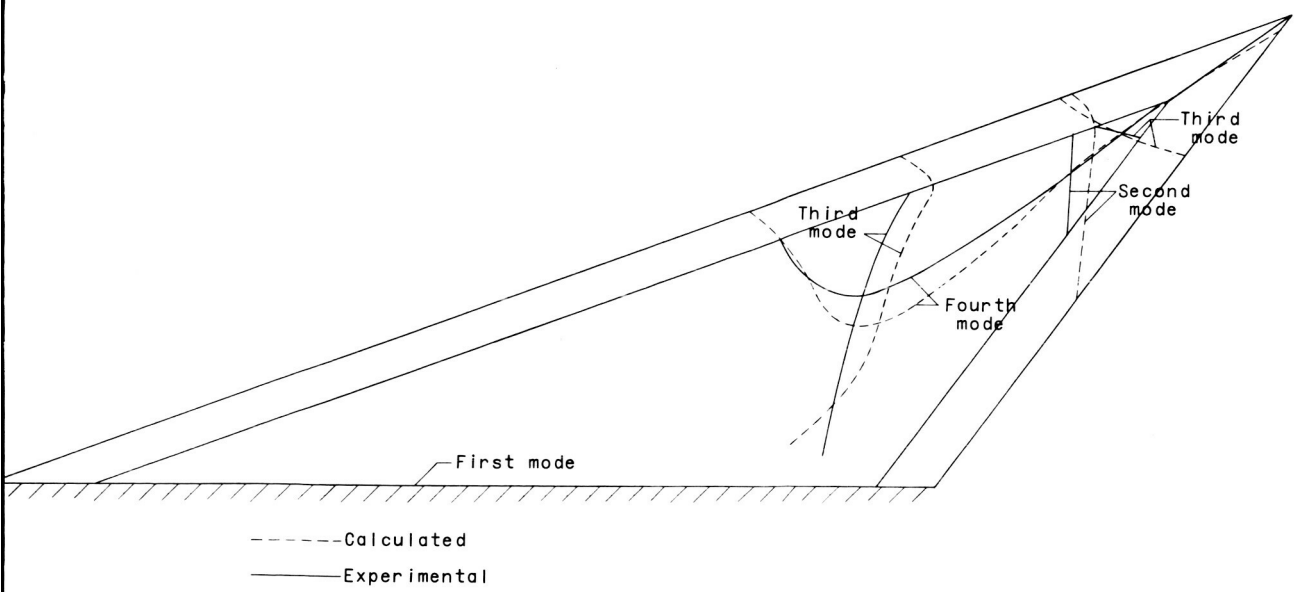

Figure 4.- Comparison of calculated and experimental node lines for a 0.125-inch-thick arrow wing.

Apparatus

Wind tunnel.- The tests were made in the Langley 9- by 6-foot thermal structures tunnel, a blowdown facility operating at a Mach number of 3 and exhausting to the atmosphere. The tunnel includes a heat exchanger which is preheated to provide stagnation temperatures from 250° F to 660° F. Dynamic pressures range from 1,300 to 5,000 pounds per square foot. Air storage capacity is sufficient to maintain full test conditions for approximately 70 seconds at the lower dynamic pressure and 40 seconds at the higher dynamic pressure. A more detailed description of the tunnel is given in the appendix of reference 6.

Boundary-layer control.- In an effort to control boundary-layer effects and assure uniform flow over the wings, the models were mounted on a reflection plane of diamond planform with half-angle bevels at the leading and trailing edges. (See fig. 5(a).) The reflection plane was located 8 inches from the tunnel floor and flow conditions were monitored by 15 static-pressure orifices. Variation in pressure over the top of the plane ranged from 12 percent above to 3 percent below theoretical values.

Model stabilization.- During the tunnel starting phase, flow separation from the nozzle walls imposed large transient loads on the models. For protection during this transient period, the wings were sandwiched between pieces of balsa and plywood and stabilized by dowels extending from an air ram at the tunnel sidewall. The stabilizing arrangement is shown in figure 5(b). No protection was provided during tunnel shutdown.

Test Procedure

The wind-tunnel tests were made at stagnation temperatures and dynamic pressures which covered the entire operating range of the tunnel. The stagnation temperature for any given test was predetermined and essentially constant. In some tests, the dynamic pressure was held constant; in other tests it was varied manually in an effort to cross the flutter boundary more than once, or to approach the boundary at a particular point. Changes in dynamic pressure were guided by observation of the model on closed-circuit television.

During the tunnel starting phase, approximately 0.2 second prior to establishment of supersonic flow, passage of the normal-shock wave released the stabilization apparatus. The dowels always released first at the tunnel walls. A beveled leading edge on the plywood forced it to open away from the test wing. Upon release, the models underwent oscillations of considerable amplitude; however, the oscillations were highly damped and nondestructive.

RESULTS AND DISCUSSION

Wing Temperatures

Temperatures were obtained at one or more points on each wing, at least until the onset of flutter. After flutter began, many of the externally mounte

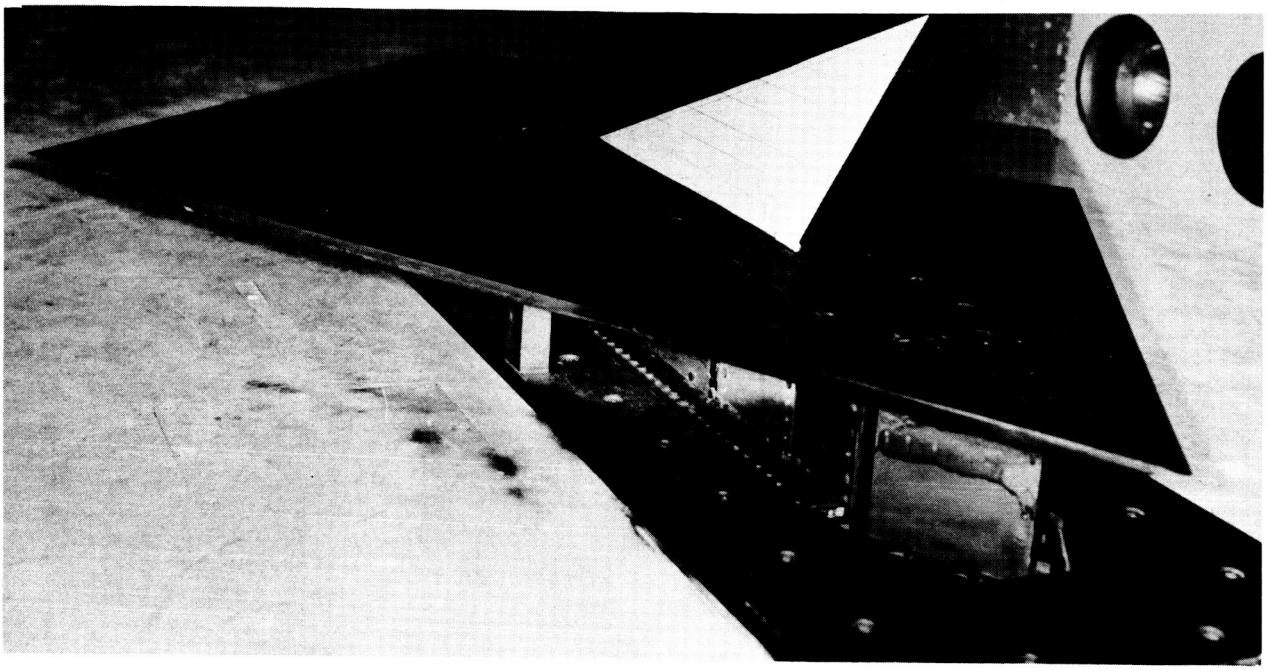

(a) Model mounted in the reflection plane. Viewed from downstream. L-61-4816

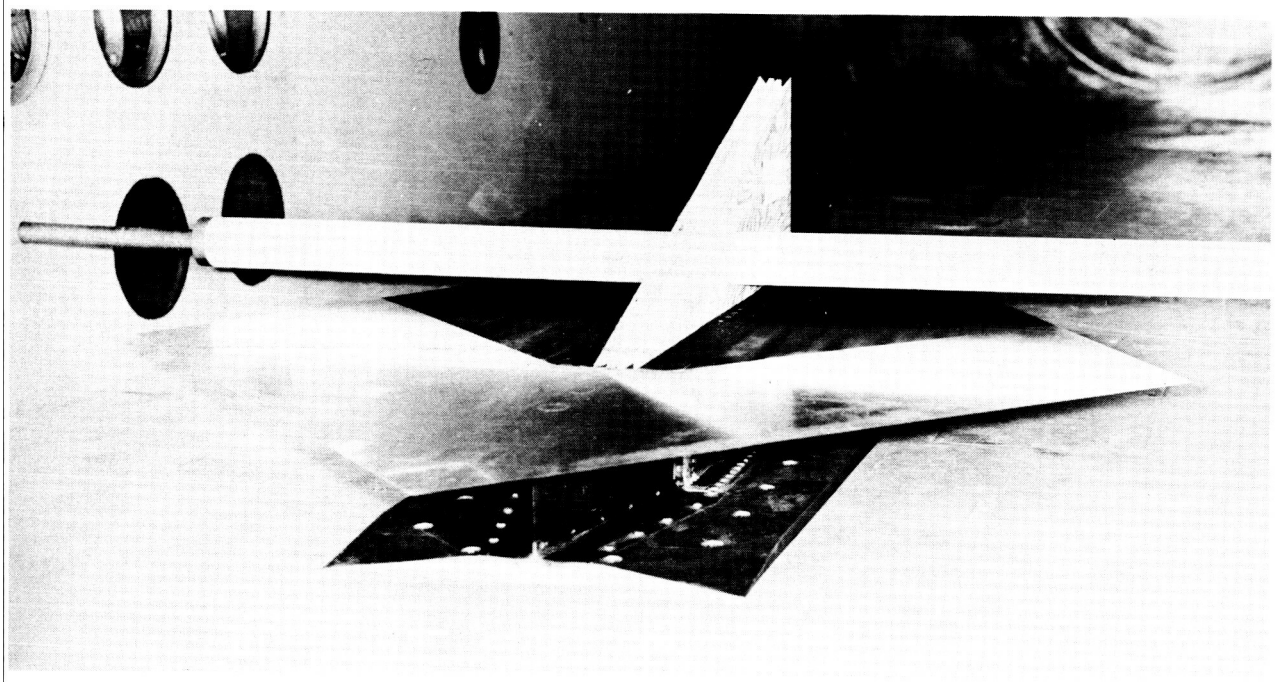

(b) Stabilized model mounted in the reflection plane. Viewed from upstream. L-61-4818

Figure 5.- Test apparatus.

thermocouples became inoperative. Temperature data from two tests are presented in table II. Data from the test on wing A6 were selected because the model was extensively instrumented and because the test was made at constant stagnation temperature and pressure just below the flutter boundary. Data from the test on wing A7 were chosen because the model had identical thermocouple instrumentation on each side of the wing (at locations 6, 8, and 13 as shown in figure 2), in order to give an indication of thermocouple reliability. This wing was tested in the flutter region at constant stagnation temperature but varying pressure.

Of the fifteen thermocouples on wing A6, only those numbered 1, 2, 4, 8, 9, 11, 12, 14, and 15 yielded useful data. Thermocouples 6 and 13 remained operative throughout the test, but apparently were interchanged and the data from them were therefore discarded.

Temperature distribution as a function of time was computed for wings A3, A5, A6, and A7, with heat-transfer coefficients obtained by the method outlined in reference 7. Each wing was divided into 50 elements as shown in figure 6. Measured and calculated temperatures for wings A6 and A7 are compared in table II. Agreement is seen to be fairly good except at the locations of thermocouples 1

TABLE II.- TEMPERATURE DATA

(a) Wing A6

Time, sec	Temperature, in °F, for thermocouple -																	
	1		2		4		8		9		11		12		14		15	
	Meas.	Calc.	Meas.	Calc.	Meas.	Calc.	Meas.	Calc.	Meas.	Calc.	Meas.	Calc.	Meas.	Calc.	Meas.	Calc.	Meas.	Calc.
0	60	59	60	59	60	59	59	59	60	59	60	59	58	59	60	59	60	59
5	167	176	191	178	155	137	76	94	184	177	181	178	185	141	102	102	85	95
10	216	256	264	269	224	215	104	125	250	263	255	261	257	225	150	132	116	126
15	240	295	306	321	272	270	129	144	286	308	300	321	301	283	183	149	138	146
20	255	316	332	352	305	308	150	157	307	334	328	353	331	322	204	158	156	157
25	262	326	348	371	328	333	167	165	319	348	347	372	351	348	218	164	169	164
30	266	332	361	384	343	351	180	171	328	358	361	387	366	368	226	167	179	169
35	270	337	368	394	354	364	191	175	333	366	371	397	377	381	231	169	187	173
40	272	339	372	400	362	373	199	178	337	369	378	403	384	391	234	170	193	176

(b) Wing A7

Time, sec	Temperature, in °F, for thermocouple -								
	6			8			13		
	Meas.	Calc.	[a]Meas.	Meas.	Calc.	[a]Meas.	Meas.	Calc.	[a]Meas.
0	64	65	64	65	65	65	65	65	65
5	186	193	189	98	132	106	176	180	175
10	282	295	284	137	175	146	261	273	261
15	336	347	338	160	189	168	307	321	307
20	381	394	382	181	204	191	352	362	350
25	419	433	428	200	220	210	388	399	387
30	437	452	442	208	221	218	405	415	405
35	452	469	460	216	224	226	419	429	420
40	462	482		224	228	234	431	440	432
45	471	491		230	231	240	440	449	441
50	476	498		236	237	246	446	457	448
55	479	501		240	240	250	450	461	452
60	479	500		243	241	253	451	462	453
65	474	494		245	241	255	449	459	451

[a]Measured by thermocouple on opposite side.

and 14 on wing A6, where the grid spacing used in the calculation prevented realistic transient temperature response of elements 1 and 2. (See fig. 6.) A description of the method used for the calculations is given in the appendix.

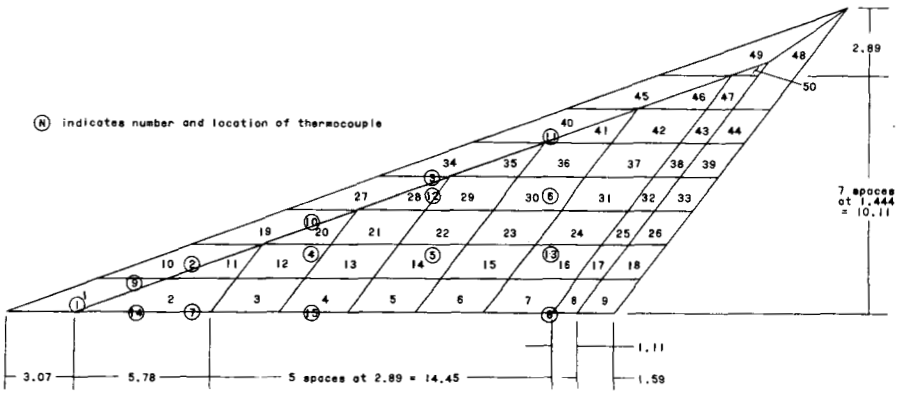

Figure 6.- Fifty-element grid used for calculation of temperature distribution. Linear dimensions are in inches.

Flutter Data

Flutter data are presented in table III. Shown in figure 7 is a plot of the flutter-velocity index $\frac{V}{b\omega_\alpha\sqrt{\mu}}$ against the wing temperature rise ΔT. The

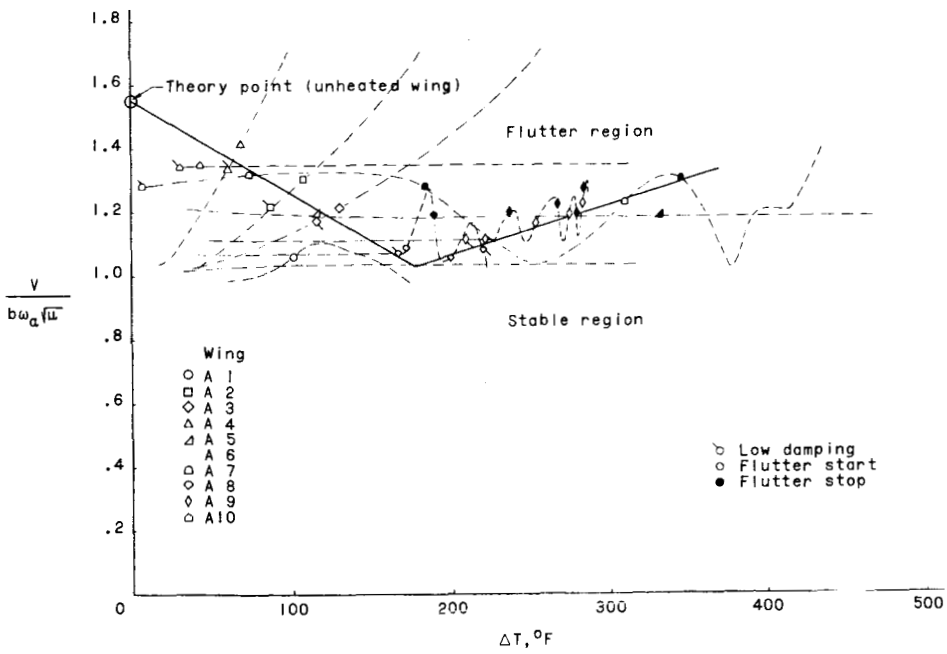

Figure 7.- An experimental flutter boundary for a 0.125-inch-thick flat-plate arrow wing showing the effect of aerodynamic heating.

TABLE III.- FLUTTER DATA

Wing	Time, sec	Free-stream velocity, fps	Free-stream density, slugs/cu ft	Calc. wing temp. 12 in. from L.E., °F	Temp. rise 12 in. from L.E., °F	Exp. third nat. freq., cps (a)	Exp. flutter freq., cps (b)	Free-stream dynamic pressure, lb/sq ft	Mass-density parameter	Stagnation temp., °F (c)	Flutter-velocity index with - Calc. ω_α	Flutter-velocity index with - Exp. ω_α
0.125-inch-thick wing												
A1	1.0 - 10.0	2127 - 2616	0.000524 - 0.000471	82 - 182	0 - 100	139	No flutter	733 - 1612	158 - 109	327 - 427	0.72 - 1.06	0.73 - 1.08
	10.0 - 20.0	2616 - 2601	.000471 - .000393	182 - 255	100 - 173	139	55	1612 - 1329	109 - 131	427 - 416	1.06 - .96	1.08 - .98
A2	1.0 - 10.0	2219 - 2505	0.000431 - 0.000639	85 - 170	2 - 87	139	No flutter	1061 - 2099	119 - 77	296 - 353	0.86 - 1.21	0.88 - 1.23
	10.0 - 12.5	2505 - 2505	.000639 - .000779	170 - 191	87 - 108	139	Low damping	2099 - 2444	77 - 66	353 - 352	1.21 - 1.30	1.23 - 1.33
	12.5 - 30.0	2505 - 2493	.000779 - .001518	191 - 277	108 - 194	139	71	2444 - 4717	66 - 34	352 - 346	1.30 - 1.81	1.33 - 1.84
A3	1.0 - 10.0	2180 - 2633	0.000363 - 0.000577	85 - 199	1 - 115	140	No flutter	863 - 2000	141 - 89	383 - 434	0.78 - 1.18	0.78 - 1.19
	10.0 - 11.3	2633 - 2634	.000577 - .000613	199 - 213	115 - 130	140	Low damping	2000 - 2126	89 - 84	434 - 436	1.18 - 1.21	1.19 - 1.23
	11.3 - 32.0	2634 - 2634	.000613 - .001338	213 - 357	130 - 273	140	60	2126 - 4641	84 - 38	436 - 431	1.21 - 1.80	1.23 - 1.82
A4	1.0 - 12.4	2180 - 2356	0.000436 - 0.000914	83 - 147	4 - 60	142	No flutter	1036 - 2537	118 - 56	239 - 260	0.85 - 1.33	0.85 - 1.33
	12.4 - 14.3	2356 - 2355	.000914 - .001031	147 - 156	60 - 69	142	Low damping	2537 - 2859	56 - 50	260 - 259	1.33 - 1.41	1.33 - 1.41
	14.3 - 27.0	2355 - 2344	.001031 - .001715	156 - 194	69 - 107	142	75	2859 - 4711	50 - 30	259 - 243	1.41 - 1.81	1.41 - 1.81
A5	1.0 - 5.0	2390 - 2900	0.000450 - 0.000481	82 - 190	8 - 116	142	No flutter	1285 - 2033	114 - 107	498 - 631	0.95 - 1.19	0.94 - 1.18
	5.0 - 19.0	2900 - 2915	.000481 - .000471	190 - 406	116 - 332	142	----------	2033 - 2001	107 - 109	631 - 641	1.19 - 1.18	1.18 - 1.18
	19.0 - 71.0	2915 - 2874	.000471 - .000460	406 - 548	332 - 474	142	No flutter	2001 - 1900	109 - 111	641 - 597	1.18 - 1.15	1.18 - 1.15
A6	1.0 - 63.0	2134 - 2691	0.000325 - 0.000416	60 - 400	1 - 341	133	No flutter	740 - 1506	158 - 123	341 - 479	0.72 - 1.02	0.76 - 1.09
A7	1.0 - 2.0	2234 - 2177	0.000376 - 0.000990	67 - 70	3 - 6	140	No flutter	938 - 2346	136 - 52	464 - 574	0.81 - 1.28	0.84 - 1.33
	2.0 - 4.0	2177 - 2845	.000990 - .000616	70 - 137	6 - 73	140	Low damping	2346 - 2493	52 - 83	574 - 590	1.28 - 1.32	1.33 - 1.37
	4.0 - 8.5	2845 - 2832	.000616 - .000572	137 - 248	73 - 184	140	70	2493 - 2294	83 - 90	590 - 576	1.32 - 1.26	1.37 - 1.32
	8.5 - 20.0	2832 - 2858	0.000572 - 0.000526	248 - 375	184 - 311	140	No flutter	2294 - 2148	90 - 98	576 - 599	1.26 - 1.22	1.32 - 1.27
	20.0 - 24.5	2858 - 2840	.000526 - .000609	375 - 414	311 - 350	140	Low damping	2148 - 2456	98 - 84	599 - 586	1.22 - 1.30	1.27 - 1.36
	24.5 - 62.0	2840 - 2802	.000609 - .000767	414 - 497	350 - 433	140	No flutter	2456 - 3011	84 - 67	586 - 555	1.30 - 1.45	1.36 - 1.51
A8	1.0 - 23.5	2262 - 2513	0.000387 - 0.000518	72 - 235	4 - 167	139	No flutter	990 - 1636	133 - 99	316 - 358	0.83 - 1.07	0.85 - 1.09
	23.5 - 24.5	2513 - 2514	.000518 - .000526	235 - 238	167 - 170	139	Low damping	1636 - 1662	99 - 98	358 - 360	1.07 - 1.08	1.09 - 1.10
	24.5 - 30.2	2514 - 2501	.000526 - .000635	238 - 258	170 - 190	139	55	1662 - 1986	98 - 81	360 - 346	1.08 - 1.18	1.10 - 1.20
	30.2 - 35.6	2501 - 2512	0.000635 - 0.000501	258 - 268	190 - 200	139	No flutter	1986 - 1581	81 - 102	346 - 358	1.18 - 1.05	1.20 - 1.07
	35.6 - 55.5	2512 - 2503	.000501 - .000538	268 - 289	200 - 221	139	55	1581 - 1685	102 - 95	358 - 351	1.05 - 1.08	1.07 - 1.11
	55.5 - 62.0	2503 - 2495	.000538 - .000517	289 - 290	221 - 222	139	Low damping	1685 - 1609	95 - 99	351 - 346	1.08 - 1.06	1.11 - 1.08
A9	1.0 - 18.0	2280 - 2629	0.000390 - 0.000511	78 - 263	4 - 189	138	No flutter	1014 - 1766	132 - 100	352 - 435	0.84 - 1.11	0.86 - 1.14
	18.0 - 24.8	2629 - 2628	.000511 - .000510	263 - 297	189 - 223	138	Low damping	1766 - 1761	100 - 101	435 - 435	1.11 - 1.11	1.14 - 1.14
	24.8 - 28.1	2628 - 2637	.000510 - .000608	297 - 311	223 - 237	138	54	1761 - 2114	101 - 86	435 - 439	1.11 - 1.22	1.14 - 1.25
	28.1 - 33.4	2637 - 2634	0.000608 - 0.000557	311 - 327	237 - 253	138	No flutter	2114 - 1932	86 - 93	439 - 440	1.22 - 1.16	1.25 - 1.19
	33.4 - 39.0	2634 - 2624	.000557 - .000623	327 - 342	253 - 268	138	55	1932 - 2145	93 - 82	440 - 427	1.16 - 1.22	1.19 - 1.25
	39.0 - 44.0	2624 - 2634	.000623 - .000577	342 - 349	268 - 275	138	No flutter	2145 - 2002	82 - 89	427 - 440	1.22 - 1.18	1.25 - 1.21
	44.0 - 47.1	2634 - 2620	0.000577 - 0.000620	349 - 353	275 - 279	138	59	2002 - 2141	89 - 83	440 - 426	1.18 - 1.18	1.21 - 1.24
	47.1 - 53.5	2620 - 2626	.000620 - .000620	353 - 358	279 - 284	138	No flutter	2141 - 2138	83 - 83	426 - 432	1.18 - 1.22	1.24 - 1.26
	53.5 - 57.8	2626 - 2605	.000620 - .000683	358 - 360	284 - 286	138	59	2138 - 2317	83 - 75	432 - 413	1.22 - 1.27	1.26 - 1.30
	57.8 - 61.5	2605 - 2660	0.000683 - 0.000579	360 - 359	286 - 285	138	No flutter	2317 - 2048	75 - 89	413 - 424	1.27 - 1.17	1.30 - 1.20
	61.5 - 62.8	2660 - 2613	.000579 - .000682	359 - 359	285 - 285	138	Low damping	2048 - 2328	89 - 75	424 - 424	1.17 - 1.27	1.20 - 1.30
	62.8 - 66.6	2613 - 2673	.000682 - .000694	359 - 357	285 - 283	138	59	2328 - 2479	75 - 74	424 - 392	1.27 - 1.27	1.30 - 1.30
	66.6 - 71.0	2673 - 2572	0.000694 - 0.000506	357 - 353	283 - 279	138	No flutter	2479 - 1674	74 - 101	392 - 398	1.27 - 1.08	1.30 - 1.11
A10	1.0 - 2.0	2350 - 2642	0.000530 - 0.000740	91 - 114	6 - 30	138	No flutter	1463 - 2583	97 - 69	418 - 470	1.01 - 1.34	1.04 - 1.38
	2.0 - 2.7	2642 - 2671	.000740 - .000732	114 - 126	30 - 42	138	Low damping	2583 - 2611	69 - 70	470 - 474	1.34 - 1.35	1.38 - 1.38
	2.7 - 69.0	2671 - 2563	.000732 - .000565	126 - 367	42 - 283	138	70	2611 - 1856	70 - 91	474 - 389	1.35 - 1.14	1.38 - 1.17
0.156-inch-thick wing												
B1	1.0 - 31.0	2314 - 2938	0.000350 - 0.001150	76 - 515	4 - 443	180	No flutter	939 - 4964	183 - 56	496 - 653	0.58 - 1.34	0.57 - 1.31
B2	1.0 - 25.8	2217 - 2719	0.000362 - 0.001081	86 - 356	2 - 271	180	No flutter	889 - 4000	177 - 60	381 - 494	0.57 - 1.20	0.54 - 1.18
	25.8 - 36.0	2719 - 2689	.001081 - .001208	356 - 397	271 - 313	180	Low damping	4000 - 4371	60 - 53	494 - 463	1.20 - 1.26	1.18 - 1.23
B3	1.0 - 2.6	2182 - 2937	0.000363 - 0.001051	85 - 154	1 - 66	180	No flutter	864 - 4398	176 - 61	495 - 640	0.56 - 1.27	0.55 - 1.25
	2.6 - 2.9	2937 - 2910	.001051 - .001079	154 - 169	66 - 85	180	Low damping	4398 - 4535	61 - 59	640 - 641	1.27 - 1.29	1.25 - 1.26
	2.9 - 17.3	2910 - 2915	.001079 - .001161	169 - 474	85 - 390	180	85	4535 - 4939	59 - 55	641 - 638	1.29 - 1.34	1.26 - 1.31
	17.3 - 20.0	2915 - 2908	.001161 - .001167	474 - 494	390 - 410	180	Low damping	4939 - 4939	55 - 55	638 - 635	1.34 - 1.34	1.31 - 1.31
	20.0 - 32.0	2908 - 2828	.001167 - .001087	494 - 520	410 - 436	180	No flutter	4939 - 4346	55 - 59	635 - 551	1.34 - 1.25	1.31 - 1.22
B4	1.0 - 37.0	2184 - 2807	0.000435 - 0.001172	60 - 484	2 - 426	180	No flutter	1037 - 4618	147 - 55	473 - 557	0.61 - 1.29	0.60 - 1.26

[a]The third natural frequency was taken as the average value when it was not determined experimentally; i.e., table I shows that the frequency for wing A1 was not obtained; therefore, the value shown is the average value of 139 cps.

[b]Frequency is that existing at beginning of flutter period.

[c]Stagnation temperature approached the average test value in approximately 3 seconds; e.g., for test A6, the stagnation temperature reached 468° in 3 seconds.

value of ω_α was taken as the calculated value of the third natural frequency of the unheated wing. The mass-density parameter μ is the ratio of the mass of the wing to the mass of a volume of air enclosing the wing. The volume of air is that of a cone with a base diameter equal to the root chord and an altitude equal to the semispan. The temperature rise ΔT is the calculated increase in temperature at a point 12 inches from the leading edge, conduction being neglected. This temperature rise would correspond approximately to the calculated temperature rise of element 23 (see fig. 6) even if conduction were taken into account. Heat transfer was computed according to reference 7, with turbulent flow being assumed.

Experimental flutter points were determined from the strain-gage records and the high-speed motion pictures. The strain-gage records contain three distinct areas, illustrated in figure 8, where portions of a typical record (wing A3) are reproduced. The first area (fig. 8(a)) represents no flutter, in which only a small response, possibly due to tunnel turbulence, is recorded. The second area (fig. 8(b)) indicates low damping immediately preceding or following flutter.

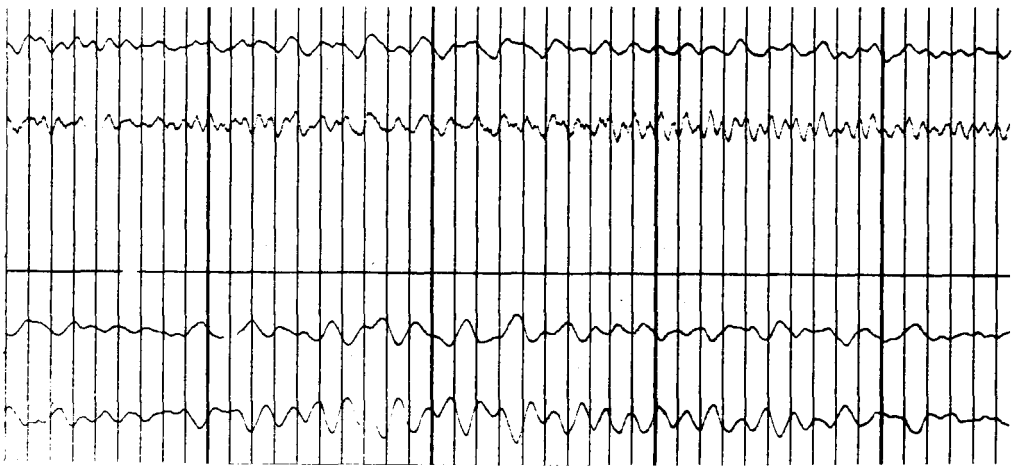

(a) No flutter.

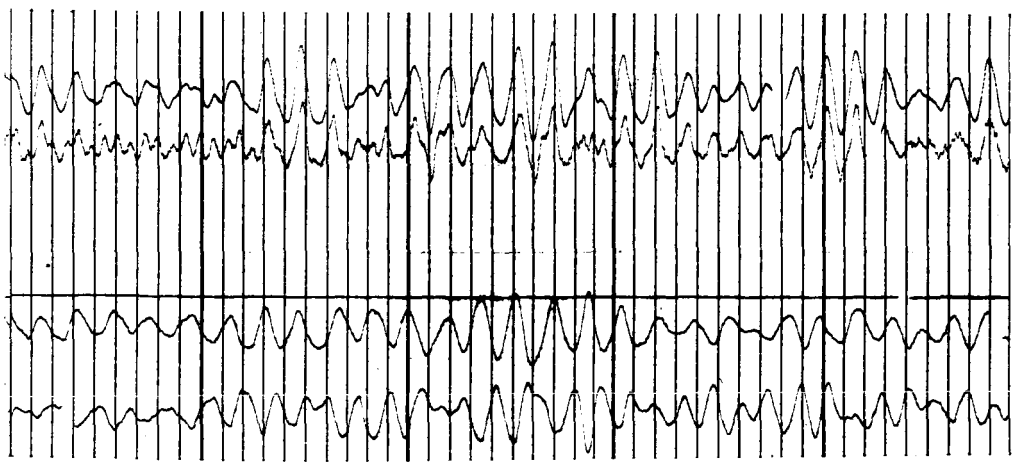

(b) Low damping.

Figure 8.- Typical oscillograph record.

Low damping was characterized by short periods of model response. The third area (figs. 8(c) and 8(d)) shows flutter, discernible by the larger amplitude and the sustained nature of the response. Two types of flutter are shown, harmonic and nonuniform. The harmonic motion appeared on the record much like a sine wave and in the motion pictures as a steady oscillation from side to side. The nonuniform motion appeared as a cyclic irregular trace, and in the motion pictures as a large-amplitude whipping action accompanied by a higher frequency vibration of small amplitude at the neutral position. Both the harmonic and the nonuniform motions were interpreted as flutter.

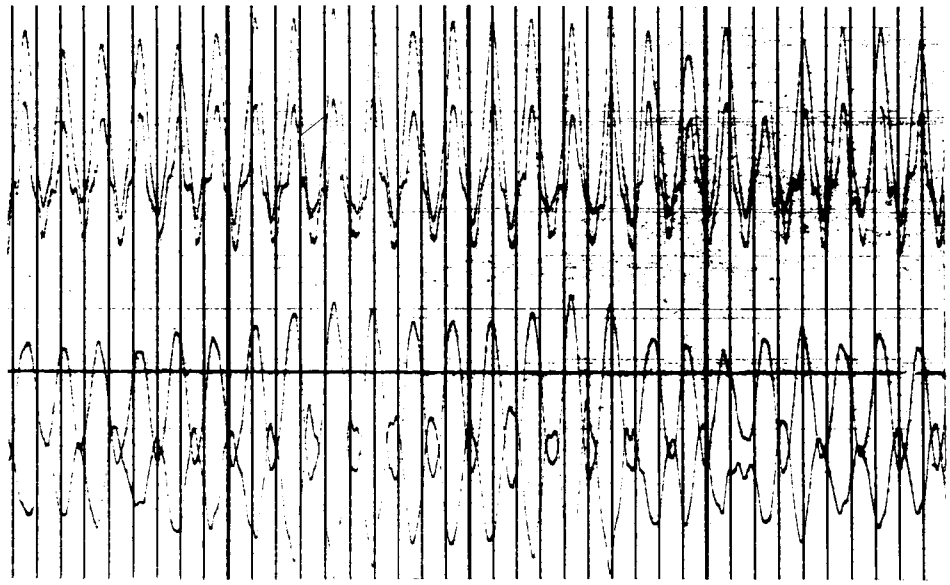

(c) Harmonic flutter.

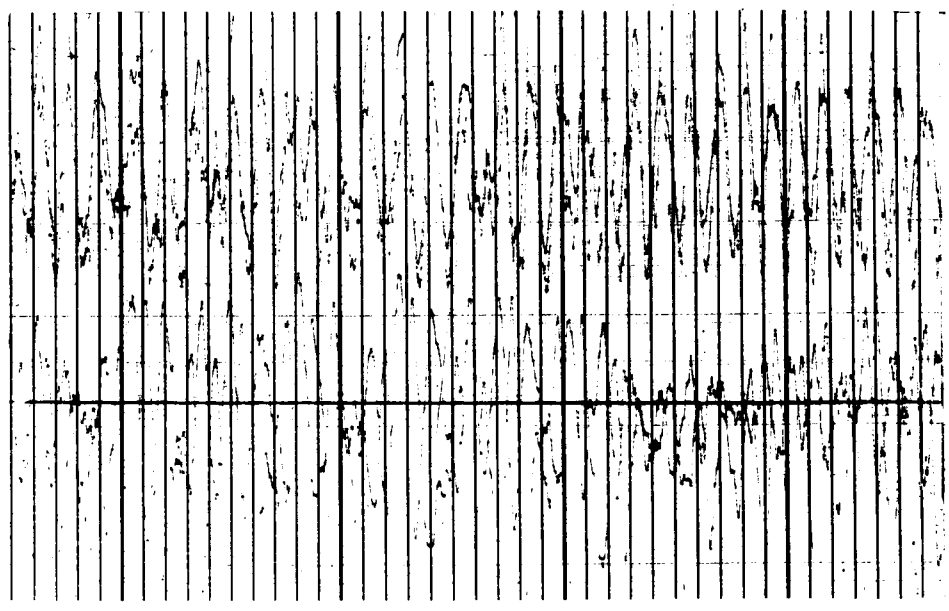

(d) Nonuniform flutter.

Figure 8.- Concluded.

Initial tests were made to determine the approximate location of the flutter boundary (see fig. 7) by choosing temperatures and dynamic pressures to cover the entire operating range of the tunnel. Once the general position of the flutter boundary became apparent, both the temperature and pressure were held constant, during some tests, to keep the number of variables to a minimum. Since the flutter-velocity index is a function of the dynamic pressure, the dashed lines in figure 7 indicate the pressure histories of each test. Open symbols indicate the beginning of low damping and flutter, and closed symbols indicate points at which flutter stopped. The solid faired line was drawn from the theoretical point for the unheated wing through the field of flutter points to indicate the approximate location of the flutter boundary. As the temperature rose, the flutter-velocity index at the boundary dropped. This result indicated that when aerodynamic heating induced thermal stress, a lower dynamic pressure was required for flutter. The effect was quite severe. The figure shows that aerodynamic heating may lower the flutter-velocity index by as much as one-third. At a temperature rise beyond 175° F, the experimental data showed that the flutter boundary had a rising trend, indicating the transient nature of the flutter response and that thermal-stress changes permitted some recovery of wing stiffness so that greater dynamic pressure was required to induce or maintain flutter.

A qualitative insight into the effect of aerodynamic heating on flutter can be gained by an examination of the isothermal plots of figure 9. The plots show calculated temperatures for wings A3 and A5, with turbulent flow assumed to exist over the entire wing surface. Superimposed in each figure is a diagram relating the plot to the experimental flutter boundary. Each set of figures shows the same effect of aerodynamic heating. Early in the test the thermal gradients between the interior of the wing and the leading and trailing edges increased, as indicated by the number and spacing of the isotherms. These thermal gradients caused high compressive stresses to exist in the areas along the leading and trailing edges while the central portion of the wing remained relatively cool. Such stress distribution has been shown in reference 8 to result in a loss of wing stiffness - a condition favorable to the onset of flutter.

The pressure and temperature histories for the tests of wings A3 and A5 were different, but in both cases flutter occurred at a time when the temperature distribution and thermal gradients were similar. Wing A3 fluttered continuously after the flutter point was reached, even though the temperature distribution changed considerably. Such behavior is due to the dependence of the flutter phenomenon on both the thermal loading and the dynamic pressure. In this test, the dynamic pressure increased as the test progressed. (See fig. 7.) During the test on wing A5, flutter began at 5 seconds and stopped at 19 seconds, even though the dynamic pressure remained constant. The temperature distribution at 5 seconds resulted in a stress pattern which caused a reduction in wing stiffness; whereas, at 19 seconds, stiffness was regained and flutter stopped. Comparing the temperature distribution at 5 seconds to that at 20 seconds and 30 seconds, it is seen that although the gradient at the leading edge has changed very little, the gradient normal to the trailing edge, and hence the thermal stress in this region, has been reduced. The temperature gradients normal to the wing root increased throughout the test and may have contributed to the increased stiffness which caused flutter to stop.

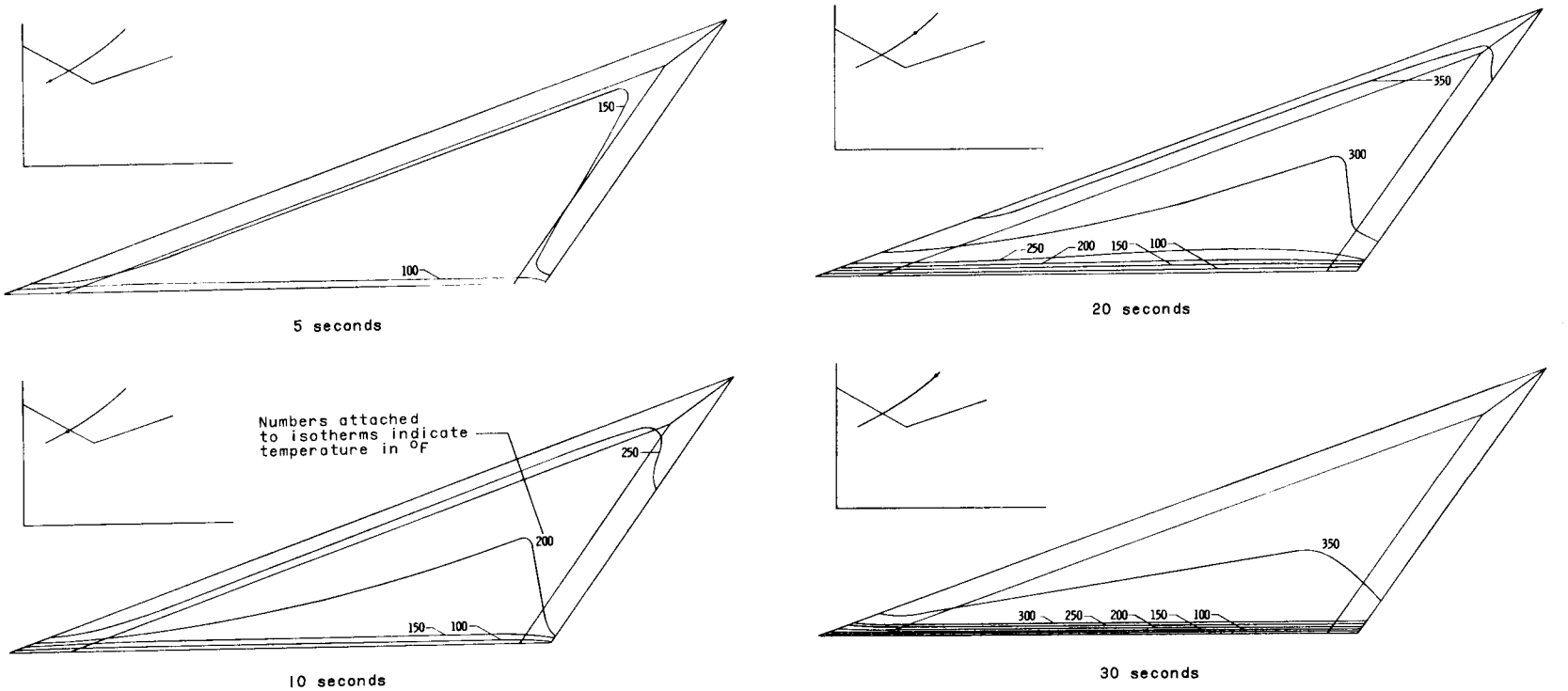

(a) Wing A3. $T_t = 436^{\circ}$ F.

Figure 9.- Calculated temperature distributions at various stages of testing.

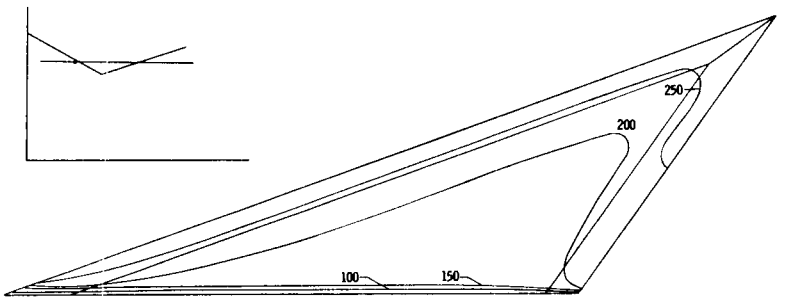

5 seconds

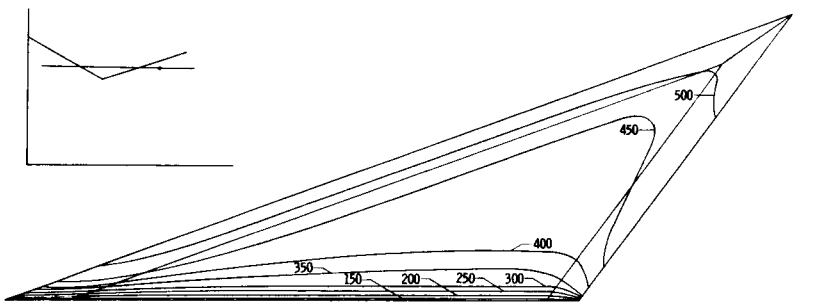

20 seconds

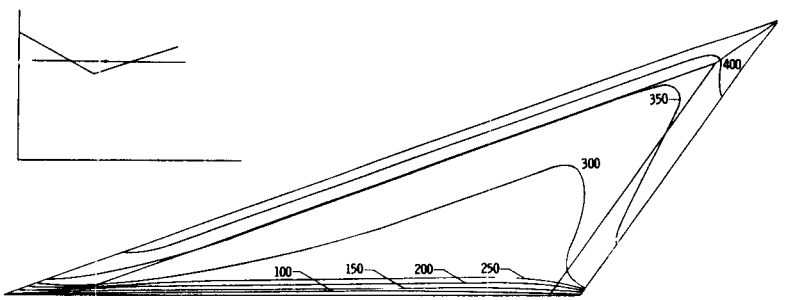

10 seconds

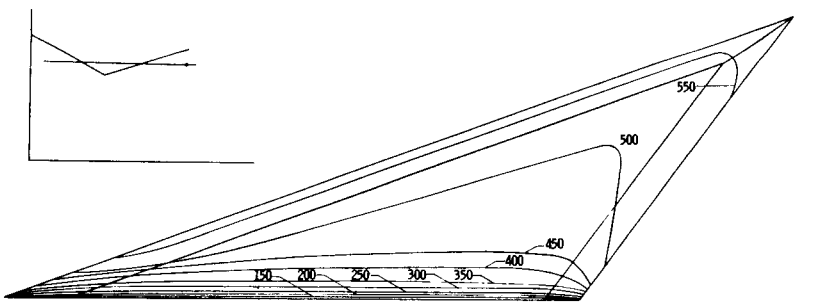

30 seconds

(b) Wing A5. T_t = 631° F.

Figure 9.- Concluded.

Reference 5 gives a procedure for calculating the flutter boundary for thin wings at supersonic speeds. A brief outline of the method is given in the last section of the appendix. This method was used to compute flutter boundaries for both the 0.125-inch-thick and 0.156-inch-thick wings. The first four calculated natural modes and frequencies for the unheated wing were used in the analysis. The boundaries are plotted in figure 10. Experimental flutter points are shown in the same graph for comparison. Since the calculated flutter boundary did not include the effect of thermal stress, the discrepancy between the theoretical boundary and the experimental flutter points is attributed largely to the effect of aerodynamic heating. Attached to each experimental point is a number showing the stagnation temperature at which the test was made. The separation of the experimental points from the calculated flutter boundary is not necessarily proportional to the stagnation temperature. The stagnation temperature is at least roughly related to the heating rate to which a model is subjected and, thus, to the maximum level of thermal stress. The intensity and distribution of such stress, however, varies continuously throughout a test and, in many cases, flutter may start at times when the stress level is not at its maximum value.

Unfortunately, the tunnel in which the tests were conducted could not be operated at stagnation temperatures below 250° F; therefore, a direct check on the unheated flutter boundary could not be obtained. However, the theoretical boundary compares reasonably well even with the experimental values for the heated wings. Since the absence of heating would increase the magnitude of the

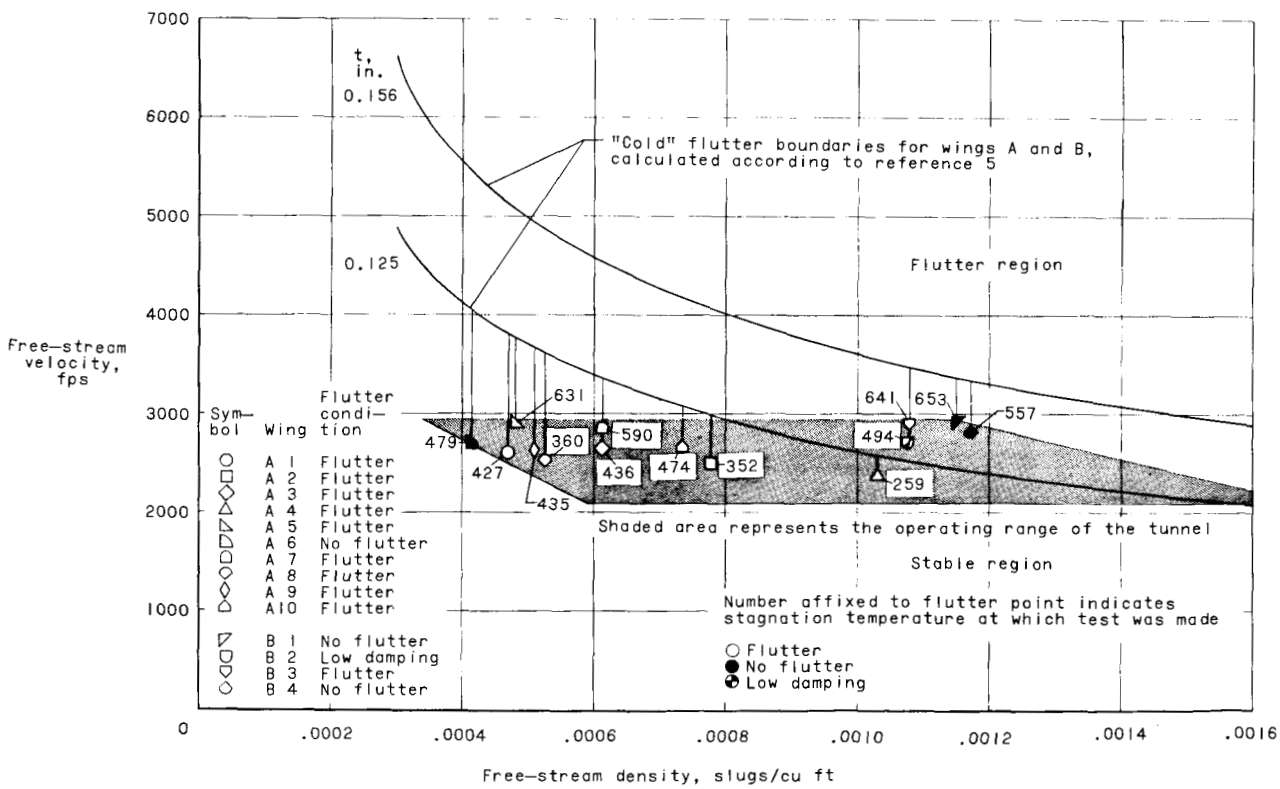

Figure 10.- Comparison of calculated and experimental flutter boundaries for wings A and B.

stable region, it may be expected that if the effect of heating were eliminated from the experimental data, agreement would be further improved.

CONCLUDING REMARKS

A series of tests has been made at a Mach number of 3 in a heated wind tunnel to investigate the effect of aerodynamic heating on the flutter of flat-plate aluminum arrow wings. From the results of the tests, an experimental flutter boundary was obtained which showed that thermal stress induced by aerodynamic heating reduced the flutter-velocity index by as much as one-third. As heating continued, the flutter boundary turned upward. This rising trend indicates the transient nature of the phenomenon. Experimental wing temperatures were compared with calculated temperatures, with generally satifactory agreement.

Natural modes and frequencies for the unheated wing were computed and the results compared with measured frequencies and nodal patterns. The agreement was consistently good. The calculated modes and frequencies were used, along with piston-theory aerodynamics, to compute a flutter boundary which did not include the effect of aerodynamic heating. The result was compared to the measured flutter points which did include the effect of aerodynamic heating. The calculated flutter boundary is in reasonable agreement with the experimental results.

Langley Research Center,
National Aeronautics and Space Administration,
Langley Station, Hampton, Va., February 12, 1963.

APPENDIX

COMPUTATION METHODS

Temperature Distribution

For temperature distribution calculations, the wing was divided into 50 elements, as shown in figure 6. Heat transfer and wing temperature during any single increment of time were assumed constant within each element. Heat-transfer coefficients, based upon turbulent flow, were computed by the method of reference 7 for flat plates by using the equation

$$h = \frac{0.144 k N_{Pr} N_{Re}^{s}}{x\left(\log_{10} N_{Re}\right)^{2.45}}$$

where k, N_{Pr}, N_{Re}, and s are evaluated at the reference temperature T^* where

$$T^* = T_e + 0.5(T_w - T_e) + 0.22(T_r - T_e)$$

Then a heat-balance equation of the form

$$h_n S_n\left(T_{aw} - \frac{T'_n + T_n}{2}\right) + \sum k_w \frac{A_{m-n}}{l_{m-n}}\left(T_m - T_n\right) = \frac{c\rho t S_n}{\tau}\left(T'_n - T_n\right)$$

was written for each element. The summation in the second term means that a term of the type shown was included for each element adjoining element n. The time increment τ was taken as 1 second. The clamping blocks at the root were assumed to be equivalent to an infinite heat sink. Repeated solutions of the heat-transfer and heat-balance equations yielded the temperature of each element at the end of each time increment.

Vibration Calculations

In order to calculate the natural modes and frequencies, the wing was divided into 37 elements as shown in figure 11. (Only 28 elements are numbered inasmuch as the 9 elements bordering the root are assumed not to deflect.) The mass of each element was assumed to be concentrated at a point which fitted into a uniform grid. The mode was assumed to be represented by the deflections of the grid points. The "total potential energy" of the wing, defined as the difference between the internal strain energy and the external work due to inertial loading, was expressed in terms of the unknown deflections of the grid points. Minimization of the total potential energy with respect to each of the grid-point

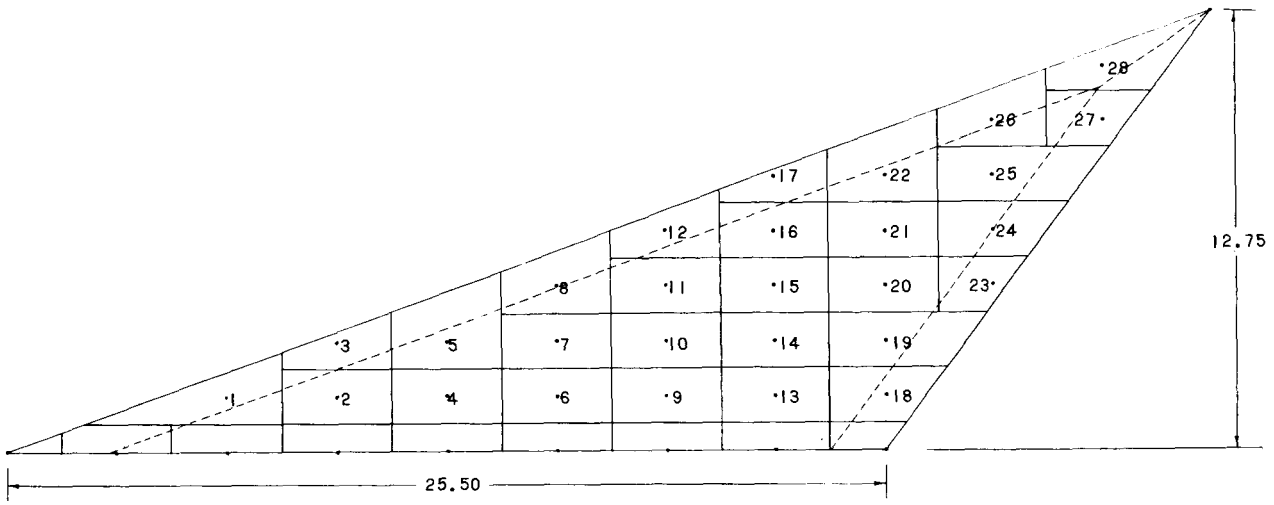

Figure 11.- Grid used for calculation of natural vibration modes and frequencies.

deflections, one at a time, yielded a set of equations (one equation for each grid point) which were solved simultaneously for the unknown grid-point deflections and associated frequencies. The solution is based upon the assumption of harmonic motion. Many details of the work are omitted here; this discussion is intended merely to outline the principles applied. A much more complete description of the method is given in reference 4.

Reference 4 makes no provision for variable thickness, such as existed on the beveled leading and trailing edges of the wings studied in this report. Some trial calculations showed that the beveled edges did not significantly affect the frequencies, but that they had to be taken into account if accurate mode shapes were to be obtained. The beveled edges were accounted for by replacing them with flat sections of the same planform, but with reduced thicknesses of such magnitude that the moment of inertia of the cross section was maintained. When this procedure was followed, the calculated nodes matched the experimental nodes much more closely than when the bevels were ignored. Thus it was concluded that the approximation used was adequate, at least for small deviations from the uniform plate thickness upon which the theory is based.

Flutter Calculations

In order to apply the method of reference 5 to calculate a flutter boundary, it is necessary to know the wing geometry, properties of the wing material, the aerodynamic conditions to which the wing is exposed, and, in addition, a sufficient number of the natural modes and frequencies so that the flutter mode may be depicted with reasonable accuracy by suitable combinations of the natural modes.

No attempt is made to describe the complete procedure for making flutter calculations, but the method will be outlined briefly. The wing is divided into 11 spanwise stations, and the distorted shape at each station for each natural

mode of vibration is approximated by a polynomial. The flutter mode is then assumed to be represented by some combination of the natural modes as expressed by their polynomials. Potential and kinetic energies are written in terms of the unknown deflections of the flutter mode. Aerodynamic forces also are expressed in terms of these unknown deflections according to piston-theory aerodynamics. The total energies and forces of the system are obtained by integration over the surface of the wing. These terms, along with a generalized damping force, are substituted into Lagrange's equation of motion. At this point, harmonic motion is assumed, and the further assumption is made that the damping coefficient is the same for all vibration modes. This procedure leads to a set of simultaneous equations whose size depends upon the number of natural modes of vibration considered in the analysis. From these equations, a complex flutter determinant is obtained which may be solved for the combinations of air density and velocity which are on the border line between the stable region and the flutter region. A number of solutions for different flight conditions yields a flutter boundary.

All the computations described in this appendix were performed with the aid of high-speed computing equipment.

REFERENCES

1. Rosecrans, Richard, Vosteen, Louis F., and Batdorf, William J., Jr.: Tests of Aerodynamically Heated Multiweb Wing Structures in a Free Jet at Mach Number 2 - Three Aluminum-Alloy Models and One Steel Model of 20-Inch Chord and Span With Various Internal Structures and Skin Thicknesses. NACA RM L57H01, 1957.

2. Davidson, John R., Rosecrans, Richard, and Vosteen, Louis F.: Tests of Aerodynamically Heated Multiweb Wing Structures in a Free Jet at Mach Number 2 - Four Aluminum-Alloy Models of 20-Inch Chord and Span With 0.064-Inch-Thick Skin, 0.025-Inch-Thick Ribs and Webs, and Zero, One, Two, or Three Chordwise Ribs. NACA RM L57L13, 1958.

3. Runyan, Harry L., and Jones, Nan H.: Effect of Aerodynamic Heating on the Flutter of a Rectangular Wing at a Mach Number of 2. NASA TN D-460, 1960. (Supersedes NACA RM L58C31.)

4. Walton, William C., Jr.: Applications of a General Finite-Difference Method for Calculating Bending Deformations of Solid Plates. NASA TN D-536, 1960.

5. Morgan, Homer G., Huckel, Vera, and Runyan, Harry L.: Procedure for Calculating Flutter at High Supersonic Speed Including Camber Deflections, and Comparison With Experimental Results. NACA TN 4335, 1958.

6. Dixon, Sidney C., Griffith, George E., and Bohon, Herman L.: Experimental Investigation at Mach Number 3.0 of the Effects of Thermal Stress and Buckling on the Flutter of Four-Bay Aluminum Alloy Panels With Length-Width Ratios of 10. NASA TN D-921, 1961.

7. Anon.: Aerodynamic Heat Transfer Handbook - Vol. I. Doc. No. D2-9514, Boeing Airplane Co., 1961, appendix E, p. 1.1.

8. Vosteen, Louis F., McWithey, Robert R., and Thomson, Robert G.: Effect of Transient Heating on Vibration Frequencies of Some Simple Wing Structures. NACA TN 4054, 1957.

NASA-Langley, 1963 L-1997